**Geoscientific
Model Development**

Modeling wet deposition and concentration of inorganics over Northeast Asia with MRI-PM/c

M. Kajino[1,2], M. Deushi[1], T. Maki[1], N. Oshima[1], Y. Inomata[3], K. Sato[3], T. Ohizumi[3], and H. Ueda[4]

[1]Meteorological Research Institute, Japan Meteorological Agency, 1-1 Nagamine, Tsukuba, 305-0052, Japan
[2]Pacific Northwest National Laboratory, P.O. Box 999 Richland, WA 99352, USA
[3]Asia Center for Air Pollution Research, 1182 Sowa, Nishi, Niigata, 950-2144, Japan
[4]Toyohashi Institute of Technology, 1-1 Hibarigaoka, Tempaku, Toyohashi 441-8580, Japan

Correspondence to: M. Kajino (kajino@mri-jma.go.jp)

Abstract. We conducted a regional-scale simulation over Northeast Asia for the year 2006 using an aerosol chemical transport model, with time-varying lateral and upper boundary concentrations of gaseous species predicted by a global stratospheric and tropospheric chemistry-climate model. The present one-way nested global-through-regional-scale model is named the Meteorological Research Institute–Passive-tracers Model system for atmospheric Chemistry (MRI-PM/c). We evaluated the model's performance with respect to the major anthropogenic and natural inorganic components, SO_4^{2-}, NH_4^+, NO_3^-, Na^+ and Ca^{2+} in the air, rain and snow measured at the Acid Deposition Monitoring Network in East Asia (EANET) stations. Statistical analysis showed that approximately 40–50 % and 70–80 % of simulated concentration and wet deposition of SO_4^{2-}, NH_4^+, NO_3^- and Ca^{2+} are within factors of 2 and 5 of the observations, respectively. The prediction of the sea-salt originated component Na^+ was not successful at near-coastal stations (where the distance from the coast ranged from 150 to 700 m), because the model grid resolution ($\Delta x = 60$ km) is too coarse to resolve it. The simulated Na^+ in precipitation was significantly underestimated by up to a factor of 30.

1 Introduction

Atmospheric chemical transport models have been important for the analysis of the emission, long-range transport, transformation, and deposition of air pollutants and climate forcing agents and are extensively used for scientific as well as regulatory purposes. Because large discrepancies remain between the model results and observational data, numerous ongoing efforts focus on model development and application. Asia is the most populated region in the world, and its associated anthropogenic emissions are huge (Ohara et al., 2007; Kurokawa et al., 2009; Zhang et al., 2009). In addition to these anthropogenic emissions, massive amounts of Asian dust particles are lofted from arid and semi-arid regions of the Asian continent.

Recently, to develop a better common understanding of the performance and uncertainties of chemical transport models in applications in East Asia, the Model Intercomparison Study Asia Phase II (MICS-Asia II) was performed (Carmichael et al., 2008). The project included nine different models and compared each model with observations and with all of the other models to evaluate model performance for ozone (O_3) and its related chemical species (Han et al., 2008), for secondary inorganic components, such as sulfate, nitrate, and ammonium (Hayami et al., 2008), and for dry and wet deposition (Wang et al., 2008). One of the major findings of the project is that an ensemble mean prediction (which is a simple average of all of the model results) agrees best with observational data. However, the discrepancies between observational data and the results of each model are sometimes very large, especially for the amount of wet deposition of sulfate, nitrate, and ammonium. For example, some differences were one to two orders of magnitude for the monthly values (Wang et al., 2008). These discrepancies were likely caused by large uncertainties in modeling wet deposition processes. Several modeling studies still lack any evaluation of
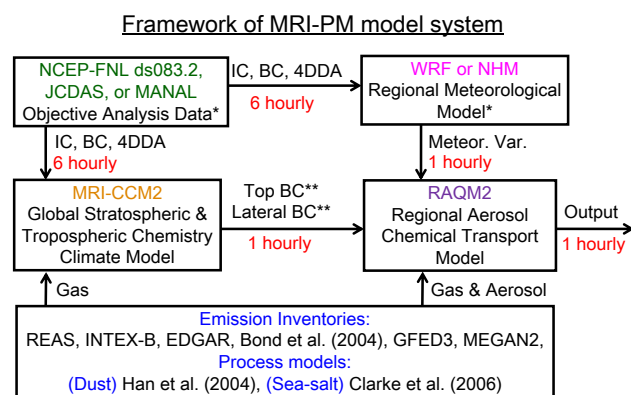
predicted amounts of wet deposition. Such an evaluation is, however, indispensable to assess the consistency in the entire modeling system, from emissions and transport to transformation and deposition.

To accurately simulate the fate of Asian air pollutants, a model (Regional Air Quality Model 2; RAQM2) has been developed with the following components: emissions of anthropogenic trace species; biomass burning; biogenic and natural (Asian dust and sea salt) aerosol emissions; advection and turbulent diffusion; photochemistry and new particle formation; gas-to-particle conversion of inorganic and organic compounds; Brownian coagulation; CCN and IN activation and cloud microphysical processes; grid-scale liquid-phase chemistry in hydrometeors as well as in aerosol water; subgrid-scale convection and wet scavenging; and dry deposition of gas and particles (details are given in Kajino et al., 2012, and in the current paper). Kajino et al. (2012) showed that the modeled size distributions, such as $PM_{2.5}/PM_{10}$ of total mass and PM_1/bulk ratios of chemical components, were consistent with the observations. They used the constant climatological values for boundary conditions, and as a result the hemispheric transport and the intrusion of stratospheric O_3 may not have been well represented. In the current study, we added time-varying lateral and upper boundary concentrations of gaseous species predicted by a global stratospheric and tropospheric Meteorological Research Institute Chemistry Climate model (MRI-CCM2; Deushi and Shibata, 2011) with a time resolution of 1 h. The present one-way nested global-through-regional-scale model is named MRI–Passive-tracers Model system for atmospheric Chemistry (MRI-PM/c). In Sect. 2, we describe the MRI-PM/c model and the observational data that we used. Section 3 discusses the model system performance and analysis, which was evaluated using the observational data. We summarize our major findings in Sect. 4.

2 Description of models and monitoring data

2.1 General description of MRI-PM/c and parameterizations used in the model system

Figure 1 illustrates the model framework. Three options for objective analysis data sets for the initial and boundary conditions for the climate and meteorological models include The US National Center for Environmental Prediction (NCEP) 6 h, $1° \times 1°$ final operational global analysis dataset (ds083.2, http://dss.ucar.edu/datasets/ds083.2); the Japan Meteorological Agency (JMA) Climate Data Assimilation System (JCDAS) 6 h, $1.25° \times 1.25°$, (http://jra.kishou.go.jp/JRA-25/AboutJCDAS_en.html); and the JMA Meso-Regional Objective Analysis (MANAL) data sets (3 h, 5 km × 5 km). These options are also used for the analysis nudging method. Two options for regional meteorological models include the Advanced Research Weather Research

Framework of MRI-PM model system

Fig. 1. Framework of Meteorological Research Institute–Passive-tracers Model (MRI-PM).

and Forecasting (WRF) model (version 3.1.1; Skamarock et al., 2008) and the JMA nonhydrostatic model (NHM; Saito et al., 2007). In this study, we selected WRF as a regional model driven by NCEP ds083.2 and used a global-scale stratospheric and tropospheric chemistry-climate model (MRI-CCM2; Deushi and Shibata, 2011) for a global atmospheric simulation, driven by JCDAS.

Regional Air Quality Model 2 (RAQM2; Kajino et al., 2012) offline, coupled with the regional meteorological models, incorporates major atmospheric chemical and dynamic processes, such as emissions of anthropogenic trace species, biomass burning, biogenic and natural (dust and sea salt) aerosol emissions, advection and turbulent diffusion, photochemistry and new particle formation, gas-to-particle conversion of inorganic and organic compounds, Brownian coagulation, CCN and IN activation and cloud microphysical processes, grid-scale liquid-phase chemistry in hydrometeors as well as in aerosol water, subgrid-scale convection and wet scavenging, and dry deposition of gas and particles.

RAQM2 used the emissions inventory from the regional emissions inventory in Asia (REAS; Ohara et al., 2007), which was extended to 2005 by Kurokawa et al. (2005) and which included NO_x, SO_2, NH_3, non-methane volatile organic compounds (NMVOCs), black carbon (BC), and primary organic aerosols (POA). The speciation of NMVOC was obtained from the INTEX-B inventory (Zhang et al., 2009). For data outside the Asian region, we used EDGAR3.2 (Oliver and Berdowski, 2001) for NO_x, SO_2, NMVOC, and POA, EDGAR2.0 (Oliver et al., 1999) for NH_3 (as NH_3 is not provided in EDGAR3.2), and Bond et al. (2004) for BC, respectively. We used the Global Fire Emissions Database (GFED3; Giglio et al., 2010) for open biomass burning emissions (NO_x, SO_2, NMVOCs, BC, and POA) and the Model of Emissions of Gases and Aerosols from Nature (MEGAN2; Guenther et al., 2006) for biogenic emissions of isoprene and terpenes. We followed Han

et al. (2004) for the dust deflation process and Clarke et al. (2006) for producing sea-salt (Fig. 1). As the proposed size distribution of the Clarke module is trimodal, it was modified into a unimodal distribution while preserving the number and volume concentrations with a standard deviation of $\sigma = 2$. We did not consider the surf zone emission (e.g., de Leeuw et al., 2000), as the area is not resolvable for the grid resolution of the current model setting ($\Delta x = 60$ km).

To simulate processes in the evolution of aerosol microscale properties such as chemical composition, size distribution, and mixing state, we developed a new triple-moment aerosol dynamics model (Kajino, 2011a, b; Kajino and Kondo, 2011; Kajino et al., 2012). RAQM2 enables non-equilibrium calculations of gas-to-particle mass transfers over a wide range of aerosol particle diameters, from 1 nm to supermicron particles. In RAQM2, six important parameterizations related to aerosol dynamics and wet deposition processes are implemented: (1) new particle formation; (2) activation of cloud condensation nuclei (CCN); (3) activation of ice nuclei (IN); (4) grid-scale cloud microphysics; (5) dry deposition; and (6) subgrid-scale convection and scavenging.

Figure 2 schematically illustrates the categorical approach to describing aerosol dynamics and cloud microphysics processes, taking the aerosol mixing state into consideration. The model groups aerosols into four categories: Aitken mode (ATK, diameter ~ 10 nm); accumulation mode (ACM, diameter ~ 100 nm); soot aggregates (AGR, diameter ~ 100 nm); and coarse mode (COR, diameter ~ 1 µm). The SO_2 molecule is oxidized by the OH radical in the air to form H_2SO_4 gas. Because the vapor pressure of H_2SO_4 gas is extremely low, homogeneous nucleation and condensation onto pre-existing particles occur simultaneously. RAQM2 can provide a rigorous solution to this competitive and non-equilibrium process with a short time step of 1 s. The newly formed particles, calculated using a parameterization of Kuang et al. (2008), are distributed into the ATK category (red arrow in Fig. 2), and condensation occurs on aerosols in all pre-existing categories (blue arrows in Fig. 2). Intra-category and inter-category Brownian coagulation (pink arrows in Fig. 2) were simulated with the Modal Aerosol Dynamics model for multiple Modes and fractal Shapes (MADMS) (Kajino, 2011a, b; Kajino and Kondo, 2011). A portion of the aerosols, larger than the critical diameter, is activated as CCN (green arrows in Fig. 2). The critical diameter of each aerosol category is parameterized by using the dry aerosol size distribution, hygroscopic mass, environmental temperature and humidity, and updraft velocity (Abdul-Razzak and Ghan, 2000). With regard to IN activation of aerosols, AGR and COR aerosols are activated by contact freezing and immersion freezing if their hydrophobic mass (BC, OA, dust) is larger than their hydrophilic mass (SO_4^{2-}, NO_3^-, NH_4^+, Cl^-, sea salt) using the parameterization of Lohmann and Diehl (2010) (orange arrows in Fig. 2). Portions of aerosols activated as CCN and IN are transferred
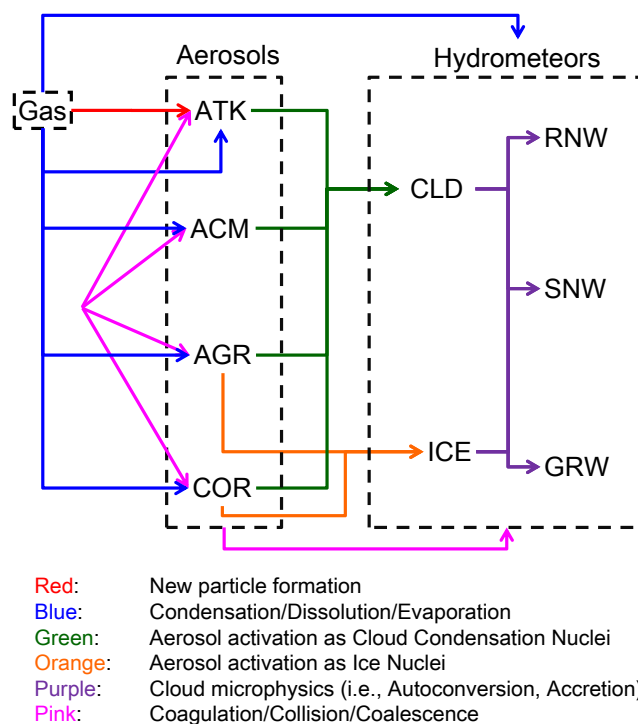

Red: New particle formation
Blue: Condensation/Dissolution/Evaporation
Green: Aerosol activation as Cloud Condensation Nuclei
Orange: Aerosol activation as Ice Nuclei
Purple: Cloud microphysics (i.e., Autoconversion, Accretion)
Pink: Coagulation/Collision/Coalescence

Fig. 2. Schematic illustration of gas-aerosol-cloud dynamic processes based on the categorical approach of RAQM2

to the cloud (CLD) and cloud ice (ICE) categories, respectively. After becoming CLD and ICE particles, the chemical components are transferred into larger hydrometeor particles, such as rain (RNW), snow (SNW), or graupel (GRW), by using the conversion rates parameterized by Lin et al. (1983) (purple arrows in Fig. 2). Aerosols in CLD and ICE that do not convert to RNW, SNW, or GRW within a time step are defined to evaporate and regenerate again after the cloud microphysics operator. The chemical components in RNW, SNW, and GRW are assumed to reach the ground surface instantaneously as wet depositions. Resuspension due to rain evaporation could be an important source of sub-cloud aerosols (Saide et al., 2012), but the current model does not consider this process. The model also considers coagulation between hydrometeors and aerosols due to gravitational settling (pink arrows in Fig. 2) and dissolution of gas into hydrometeors and aerosol water (blue arrows in Fig. 2).

The model domain, common to both WRF and RAQM2, is illustrated in Fig. 3, which also shows the locations of the observation sites of the Acid Deposition Monitoring Network in East Asia (EANET). The horizontal grid resolution is 60 km on a Lambert conformal map projection. There are 28 vertical layers from the ground to 100 hPa for WRF and 13 layers from the ground to 10 km for RAQM2 with the terrain following coordinates. Further descriptive details of the WRF-RAQM2 settings are found in Kajino et al. (2012). The output time interval of the WRF is 1 h, and thus the

Table 1. Location information for the eight EANET remote observation sites in Japan used in the study. The station locations are also shown in Fig. 3.

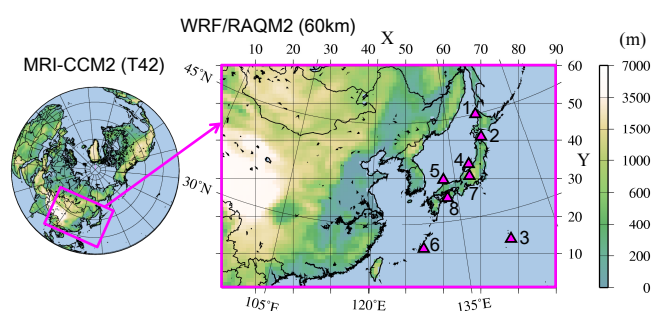|	Longitude (E)	Latitude (N)	Characteristics	Altitude (m a.s.l.)	Distance from coast (m)
1 Rishiri	141°12′	45°07′	Island	40	700
2 Tappi	140°21′	41°15′	Cape	105	360
3 Ogasawara	142°13′	27°05′	Island	230	500
4 Sado	138°24′	38°14′	Island	136	150
5 Oki	133°11′	36°17′	Cape	90	200
6 Hedo	128°15′	26°52′	Cape	60	200
7 Happo	137°47′	36°41′	Mountain	1850	*
8 Yusuhara	132°56′	33°22′	Inland	790	*

* More than 10 km from the coast.

Fig. 3. Modeling domains showing terrestrial elevation (m) and the EANET monitoring sites (triangles 1 through 8). Locations of the EANET stations are given in Table 1.

input/output time interval for RAQM2 is also 1 h. For lateral and upper boundary concentrations for the RAQM2 simulation, we used hourly concentrations of NO_x, O_3, CO, and volatile organic compounds (VOCs) that were simulated by the MRI-CCM2 with a T42 horizontal resolution (approximately 300 km). The present regional model is thus considered to be a one-way nested model of the global chemistry model (Figs. 1 and 3). The MRI-CCM2 reproduced the seasonal variations in measured O_3 concentrations at stations near the edges of the RAQM2 domain.

2.2 EANET stations and monitoring data used in the study

We used the EANET (Acid Deposition Monitoring Network in East Asia) monitoring data for model evaluation (all EANET guidelines, documents and manuals are available at http://www.eanet.cc/product.html). The EANET stations in Japan monitor 1-week (at Ogasawara) or 2-week (at other sites) accumulated concentrations of gaseous species (HNO_3, HCl, NH_3, and SO_2) and aerosol components (SO_4^{2-}, NO_3^-, Cl^-, NH_4^+, Na^+, Mg^{2+}, K^+, and Ca^{2+}) using the filter pack (FP) method. The four-stage filter pack is composed of four filters in line with the air streams entering from the bottom with a flow rate of $1 l min^{-1}$. Aerosols are collected on the bottom (i.e., first) pack with Teflon filter (pore size; 0.8 µm, diameter; 47 mm) to attain good efficiency in collecting sub-micron particles (EANET "Technical Documents for Filter Pack Method in East Asia"). By comparing the FP method with the simultaneous measurements using the Andersen sampler (a multi-stage cascade impactor), the FP method was found to efficiently collect particles up to diameters of 10 µm. The stations also monitor daily accumulated precipitation (SO_4^{2-}, NO_3^-, Cl^-, NH_4^+, Na^+, Mg^{2+}, K^+, and Ca^{2+}) using wet-only precipitation collection and ion chromatography analysis (EANET, "Technical Manual for Wet Deposition Monitoring in East Asia"), and hourly SO_2, NO, NO_x, O_3, $PM_{2.5}$, and PM_{10} concentrations, and meteorological parameters, such as wind speed, wind direction, temperature, relative humidity, and solar radiation. Quality assurance and quality control were conducted to ensure that monitoring data remained of high quality, in accordance with EANET guidelines (EANET, "Quality Assurance/Quality Control Programs").

The FP method is subject to several distinct problems when used for long-term sampling. Because of the possibility that particulate NH_4NO_3 and NH_4Cl will volatilize when collected on a filter during the 1-week or 2-week sampling period, thermodynamic equilibrium may not have been attained. In addition, high humidity can reduce the concentration of gaseous species because the filter pack traps condensed water. To avoid these artifacts, we only used total NO_3^- (T-NO_3^- is [HNO_3 gas plus NO_3^- aerosol]) and total NH_4^+ (T-NH_4^+ is [NH_3 gas plus NH_4^+ aerosol]), and gas-aerosol partitioning is not discussed in this study.

To deduce the anthropogenic SO_4^{2-} and Ca^{2+} originating from Asian dust (calcite), we defined non-sea-salt (nss) SO_4^{2-} and Ca^{2+} to exclude the contribution of sea salt using a standard mean chemical composition of seawater (DOE, 1994), as follows:

$$[\text{nss-SO}_4^{2-}] = [\text{SO}_4^{2-}] - 0.251 \times [\text{Na}^+] \qquad (1)$$

$$[\text{nss-Ca}^{2+}] = [\text{Ca}^{2+}] - 0.038 \times [\text{Na}^+] \qquad (2)$$

where [ ] denotes weight concentrations in $\mu\text{g m}^{-3}$. To distinguish the ions in precipitation from those in aerosols, we defined the precipitation ions as W-nss-SO$_4^{2-}$, W-NH$_4^+$, W-NO$_3^-$, W-nss-Ca^{2+}, and W-Na$^+$.

Among EANET stations, we selected eight remote stations in Japan for model evaluation (Fig. 3, Table 1). The island stations (Rishiri, Ogasawara, Sado, and Oki) and those on isolated capes (Tappi and Hedo) are located far from large anthropogenic emission sources in places where there are no complex, local, orographically induced winds. Thus, air pollutant transport events at these stations mostly coincide with synoptic-scale disturbances and are generally well reproduced by regional-scale models. However, because these stations are very close (< 1 km) to the ocean, regional-scale simulations of ocean-derived species such as sea salt often did not agree well with the observations. Therefore, we also included two inland stations (Happo and Yusuhara) in the model evaluation, although the wind fields at these locations can be affected by the local, mountainous topography, and the quantity of precipitation may not be predicted well by regional-scale models.

3 Results and discussion

3.1 Evaluation of aerosol chemical components

The aerosol chemical components were evaluated with the FP method; however, because the time resolution of this method is biweekly (or weekly at Ogasawara), we had only 24 (or 48) samples for each site. This limited number of samples made it difficult to evaluate transport phenomena, but we were able to evaluate the quantitative consistency of RAQM2. As explained in Sect. 2.2, we did not use gas-aerosol partitioning of semi-volatile inorganic components because of possible artifacts; however, gas-aerosol partitioning is of the utmost importance with respect to long-range transport because the dry and wet deposition rates of the gas and aerosol phases are very different (Kajino et al., 2005, 2008; Kajino and Ueda, 2007, 2011). The partitioning needs to be evaluated with other observations in the future.

We separated the observed and modeled concentrations of aerosol chemical components into near-the-coast (NC) and far-from-the-coast (FC) groups (Fig. 4) because of the different characteristics of the site locations in the regional-scale simulation framework. As we discussed in Sect. 2.2, the NC stations are located far from large anthropogenic emission sources in places where there are no complex, local, orographically induced winds, and thus air pollutant transport events mostly coincide with synoptic-scale disturbances
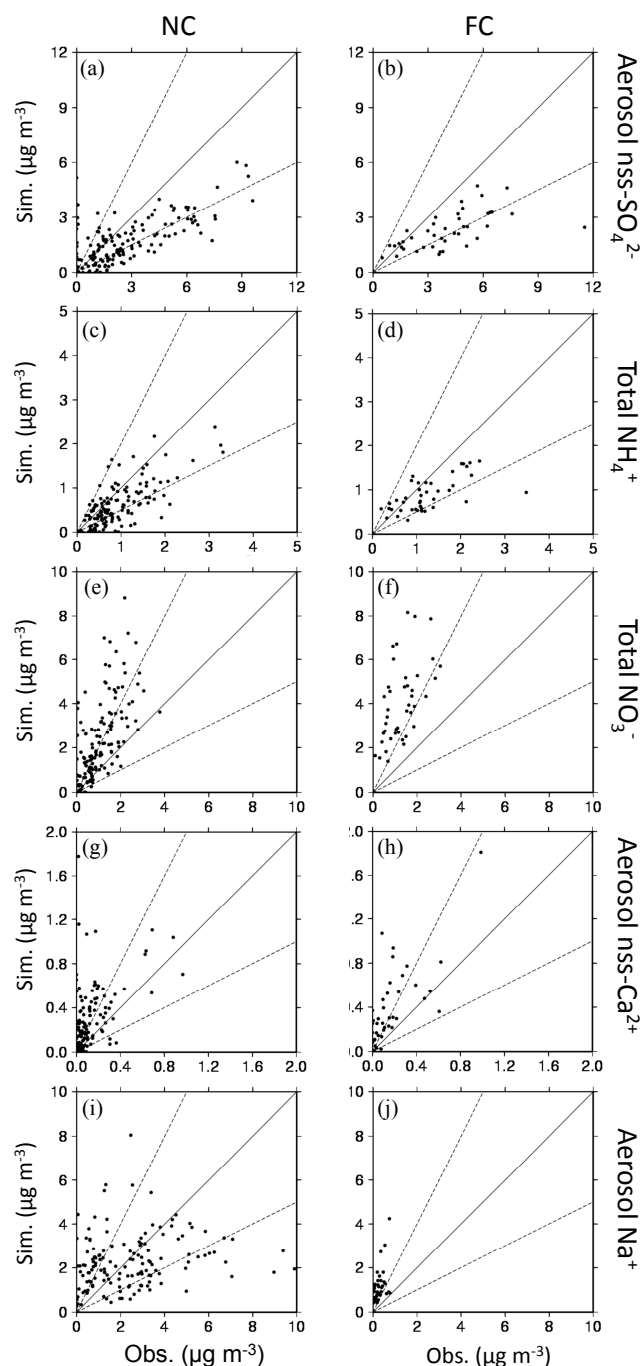

Fig. 4. Scatter diagrams of modeled vs. measured concentrations of biweekly aerosol chemical components nss-SO$_4^{2-}$, T-NH$_4^+$, T-NO$_3^-$, nss-Ca^{2+}, and Na$^+$ (top to bottom) at (left) the near-coastal stations (NC; Rishiri, Tappi, Sado, Ogasawara, Oki, Hedo) and (right) the stations far from the coast (FC; Happo and Yusuhara). Solid lines denote the 1 : 1 line, and dashed lines delimit the factor-of-2 envelope.

Table 2. Comparative statistical analysis of all observed (Obs.) and simulated (Sim.) data for the year 2006.

	Number of data	Average (Obs.)	Average (Sim.)	NMB[a]	RMSE[b]	R^2	FAC2[c]	FAC5[d]
1- or 2-week average bulk concentrations ($\mu g\,m^{-3}$)								
Nss-SO_4^{2-}	194	2.92	1.79	−0.39	2.05	0.49	0.50	0.86
T-NH_4^+	180	0.99	0.67	−0.32	0.55	0.52	0.66	0.89
T-NO_3^-	186	1.15	2.90	1.53	2.61	0.36	0.40	0.81
Nss-Ca^{2+}	194	0.14	0.30	1.24	0.31	0.50	0.33	0.69
Na^+ (NC)[e]	144	2.55	2.30	−0.10	2.25	0.07	0.46	0.86
Na^+ (FC)[f]	42	0.25	1.12	3.42	1.08	0.27	0.10	0.52
2-week average wet deposition amount ($mmol\,m^{-2}$) and precipitation amount (H_2O; mm)								
W-nss-SO_4^{2-}	192	0.82	0.50	−0.39	0.75	0.29	0.43	0.79
W-NH_4^+	192	0.80	0.65	−0.19	0.83	0.15	0.46	0.80
W-NO_3^-	192	0.82	0.92	0.13	0.83	0.25	0.54	0.86
W-nss-Ca^{2+}	192	0.38	0.20	−0.46	0.71	0.16	0.37	0.71
W-Na^+ (NC)[e]	144	16.4	1.38	−0.91	52.2	0.11	0.13	0.38
W-Na^+ (FC)[f]	48	1.01	1.03	0.022	1.50	0.23	0.42	0.75
H_2O	192	73.4	71.6	−0.025	83.6	0.18	0.49	0.86

[a] Normalized mean bias (mean bias divided by observation average). [b] Root-mean-square error. [c] Number fraction of data within a factor of 2. [d] Number fraction of data within a factor of 5. [e] Comparison of Na^+ at the near-the-coast (NC) stations (Rishiri, Tappi, Ogasawara, Sado, Oki, and Hedo). [f] Comparison of Na^+ at the far-from-the-coast (FC) stations (Happo and Yusuhara).

and are generally reproduced well by regional-scale models. However, because these stations are very close to the ocean, which is the source of sea salt particles (< 1 km, Table 1), the regional-scale simulations often did not agree well with the observations. Because the selected FC stations are also located far from large anthropogenic emission sources and far from the ocean (> 50 km), the regional-scale simulations of both anthropogenic and oceanic components should agree well with the observations. However, because wind fields can be affected by local mountainous topography, transport patterns may not always be reproduced well by regional-scale simulations. In the comparison between the observations and simulations (Table 2), we separated the NC and FC groups only for Na^+, which originated primarily from sea salt particles.

Results for the simulated and observed concentrations of anthropogenic components, such as nss-SO_4^{2-}, T-NH_4^+, and T-NO_3^-, were correlated well at both the NC and FC stations (Table 2, Fig. 4). The simulated averages of nss-SO_4^{2-} and T-NH_4^+ were approximately 30–40 % smaller than the observed averages, whereas the simulated average of T-NO_3^- was 2.5 times the observed average. Because the modeled partitioning of gases and aerosols could not be evaluated by the measurements, it was not possible to identify the reasons for the discrepancies with the available information. There were positive correlations between the simulation and observation (0.36–0.52), and the RMSEs were comparable with the averages.

We consider nss-Ca^{2+} to originate from Asian dust particles, which contain calcite. Despite the large uncertainty in

simulating dust emission flux, we were able to obtain a good value of R^2 (0.50) for nss-Ca^{2+}. Obtaining the good value was possible because all of the observation stations are situated at a distance from the extensive source regions (e.g., Taklamakan and Gobi deserts) and in the downwind region when long-range transport of Asian dust was predominant in spring and autumn of 2006.

The primary source of Na^+ is sea salt particles. Natural aerosols are usually difficult to simulate because estimates of their emission fluxes are uncertain. Whereas the averages and RMSE for Na^+ at the NC stations are similar, the correlation coefficient (R^2) at the NC stations is very low (0.07) because of the uncertainty in emission flux and because the stations are very close to the source of emission – the ocean surface. Generally, short-term (1 h) variations of modeled Na^+ concentrations are strongly correlated with observed values (such as $R \sim 0.7$ in Kajino and Kondo, 2011), because the emission mass flux of sea salt correlates strongly to the surface wind speed. The R^2 of 0.07 is low because the results are long-term averages (one or two weeks) of multiple stations with variable distances from the coast (horizontal distances from 150 to 700 m; vertical distances from 40 to 230 m). We obtained a larger R^2 for Na^+ (0.27) at the FC stations, which were far from the emission source.

3.2 Evaluation of ion concentrations in rain and snow

To evaluate the ion concentrations in precipitation, we selected the western island station Oki (Fig. 5) and the western inland station Yusuhara (Fig. 6) to illustrate differences in
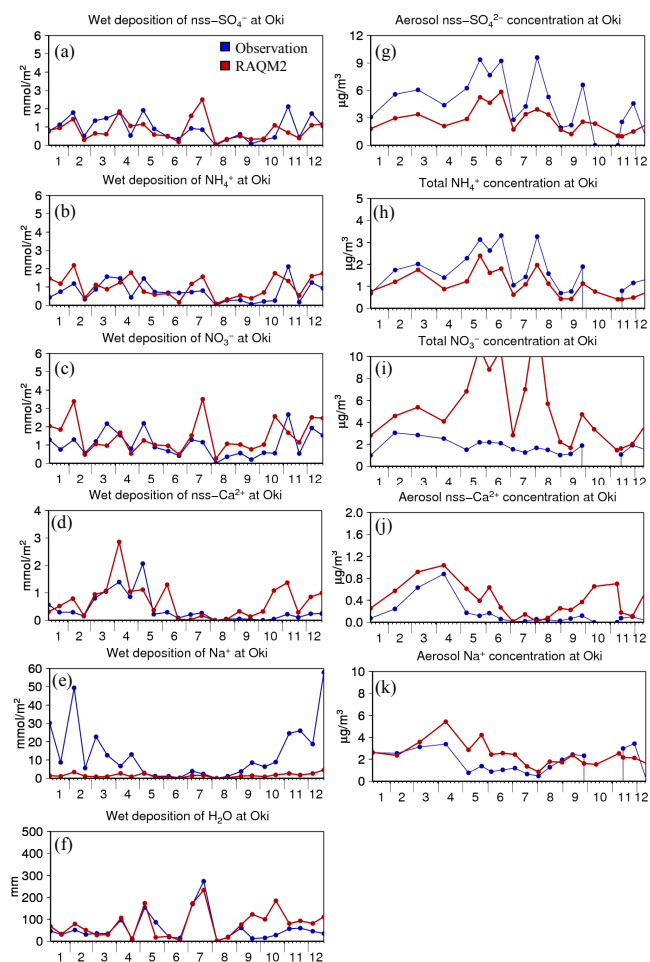
Fig. 5. Biweekly mean of daily variations of the observed (blue) and simulated (red) wet deposition at a station near the coast, Oki: **(a)** nss-SO_4^{2-}, **(b)** NH_4^+, **(c)** NO_3^-, **(d)** nss-Ca^{2+}, **(e)** Na^+, and **(f)** precipitation. Biweekly variations of the observed (blue) and simulated (red) aerosol components: **(g)** nss-SO_4^{2-}, **(h)** NH_4^+, **(i)** NO_3^-, **(j)** nss-Ca^{2+} and **(k)** Na^+.

Fig. 6. Same as Fig. 5 but at a station far from the coast, Yusuhara.

model performance for NC and FC stations. We made comparisons to the statistical results at the eight remote EANET stations (Table 2 and Fig. 7).

Both time variations and values of precipitation at Oki (Station 5) were predicted well by the model: for example, the ratio of 2-week mean simulation/observation (Sim : Obs ratio) was 1.36, and $R = 0.72$ (Fig. 7i, j). The quantities of the chemical components associated with wet deposition, most of them submicron particles such as nss-SO_4^{2-} and NH_4^+, were also predicted well at Oki (Fig. 5a, b). NO_3^- is partly attributed to submicron particles forming NH_4NO_3, while some percentage of NO_3^- also consisted of coarse (~several µm diameter) sea salt particles forming $NaNO_3$ (Kajino and Kondo, 2011; Kajino et al., 2012). As Henry's law constant of HNO_3 gas is high, the gas-phase fractions
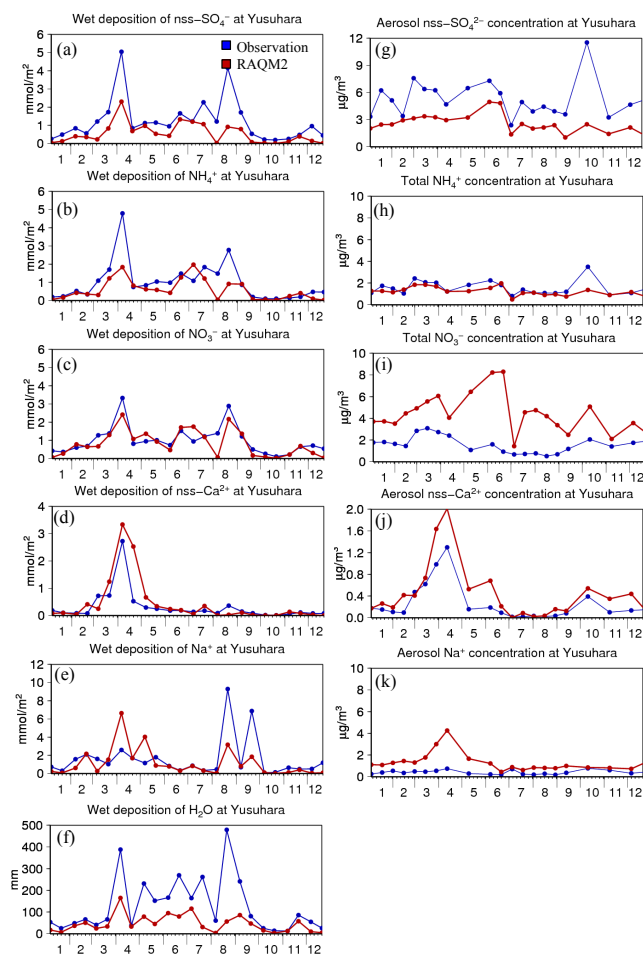
can affect the wet deposition of T-NO_3^-, too. The time variations and values of modeled NO_3^- in precipitation also agreed well with the observations (Fig. 5c).

We found the simulated wet deposition quantity of nss-Ca^{2+} to be reasonable (Fig. 5d), whereas that of Na^+ was greatly underestimated (Fig. 5e). The Sim : Obs ratios for W-Na^+ were much less than 1 at every island and cape station (Fig. 7h, Stations 1–6) and as low as 0.03 at Station 3, whereas the same ratios were much closer to 1 at inland stations (Fig. 6d and Fig. 7h, Stations 7–8).

Time variations in the precipitation at Yusuhara (Station 8) were predicted well by the model, but the amounts were underestimated (Sim : Obs = 0.36, $R = 0.69$, Fig. 7i, j). This outcome possibly resulted from an underestimation of the wet deposition of chemical components, although the model reproduced time variations well ($R > 0.7$), except for Na^+ ($R = 0.47$).

Rain accounts for the precipitation during the summer and throughout the year in western and southern Japan, whereas during the winter snow accounts for most precipitation in northern and mountainous regions. Monthly mean
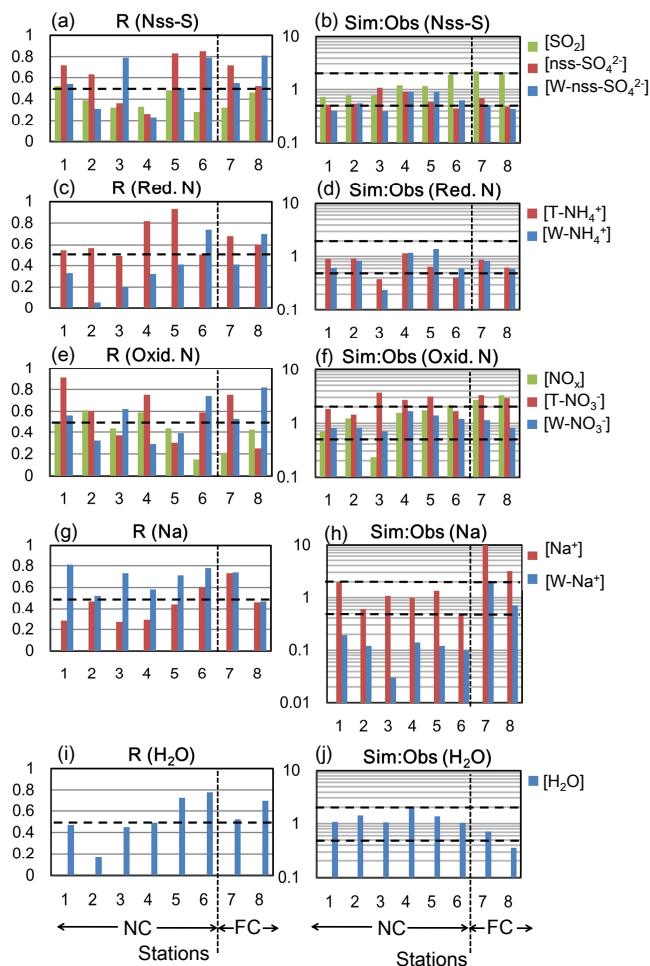
Fig. 7. Comparison of statistical results at the eight EANET stations (1. Rishiri, 2. Tappi, 3. Ogasawara, 4. Sado, 5. Oki, 6. Hedo, 7. Happo, and 8. Yusuhara). R and Sim : Obs, for gas, aerosol and precipitation of anthropogenic sulfur oxides (nss-S, **a, b**), reduced nitrogen (Red. N, **c, d**), oxidized nitrogen (Oxid. N, **e, f**), sodium (Na, **g, h**), and amounts of precipitation (H_2O, **i, j**). Dashed lines indicate (left) R of 0.5 and (right) the factor-of-2 envelope.

temperatures drop below 0 °C during the winter at Rishiri, Tappi, and Happo, and the monthly mean daily minimum temperature drops below 0 °C at Sado, Oki, and Yusuhara as well. Although the surface temperature may be above 0 °C and the surface precipitation may consist entirely of liquid water, the cloud above often harbors cold microphysical processes when the upper atmospheric temperature is below 0 °C. Because there were no large and systematic seasonal differences in the amount and ion concentrations of predicted precipitation (not shown), the formulation of wet depositional processes by RAQM2, described in Fig. 2, was consistent for both warm and cold microphysical processes.

Overall, 50 % and 80 % of the modeled and observed two-week average values of the wet deposition of anthropogenic components, such as nss-SO_4^{2-}, NH_4^+ and NO_3^-, were within

factors of two and five, respectively. This model performance is noteworthy because there have been discrepancies of 1 to 2 orders of magnitude in several regional-scale models, even for monthly mean values (Wang et al., 2008), because modeling the complexities of wet deposition processes is difficult. The predictability of natural components was worse than it was for anthropogenic components, because the fluxes of the natural emissions were heterogeneous, but the performance was good: 40 % and 70 % of the data were within factors of two and five, respectively, for the natural components. The percentages for anthropogenic components are similar to the corresponding percentages for the prediction of precipitation amounts by the regional-scale meteorological model: 49 % and 86 % were within factors of two and five, respectively.

3.3 Evaluation of the model process using the concentration and wet deposition of each component

Regression analysis of anthropogenic sulfur oxides showed similar results for nss-SO_4^{2-} aerosols, and W-nss-SO_4^{2-} in precipitation, while a somewhat lower R was obtained for SO_2 gas (Fig. 7a). The Sim:Obs ratio was greater for SO_2 than it was for the other two phases (Fig. 7b). In addition to uncertainty in SO_2 emission amount, overestimation of SO_2 is likely due to underestimation of dry deposition velocities or underestimation of the oxidation rate from S(IV) to S(VI). Because the dry deposition velocity of SO_2 is moderately fast, its underestimation may result in overestimation of the surface concentration. We formulated oxidation of SO_2 in the gas phase and in the aqueous phase of cloud, rain, and aerosol water droplets (Kajino et al., 2012). SO_2 oxidation can also occur as a heterogeneous oxidation on dust particle surfaces (Tang et al., 2004), but we did not implement this pathway in the model. In addition, we did not consider dimethyl sulfide chemistry and SO_x from outside the domain boundary in the simulation because we assumed that these components were not substantial for the targeted region. Neglect of these processes might account for the discrepancies. For sulfur oxides, approximately 50 % and 80 % of the data were within factors of two and five, respectively, at the stations.

The mean ratio of Sim:Obs for reduced nitrogen (NH_x) was similar for the air concentration and wet deposition. Of all the chemical components assessed in the study, model performance was the best for T-NH_4^+ (R^2, FAC2, FAC5 = 0.52, 0.66, 0.89, respectively). The performance was also good for [W-NH_4^+] at those stations (Stations 5–8) where the R^2 of precipitation was good (> 0.5).

Regarding the simulated oxidized nitrogen compounds (NO_x, T-NO_3^- and W-NO_3^-), T-NO_3^- was overestimated, whereas W-NO_3^- values were reasonable. The overestimation of T-NO_3^- was most likely due to overestimation of photochemical production or underestimation of the dry and wet deposition rates of T-NO_3^-. As discussed above, the dry deposition velocity of highly reactive HNO_3 gas is fast and can

be two orders of magnitude faster than that of the aerosol phase. Hence, discrepancies in the simulated deposition velocities or gas-aerosol partitioning will cause discrepancies in surface concentrations. The model performance for oxidized nitrogen was also good, and approximately 40 % and 80 % of these data were within factors of two and five, respectively, of the observations at all of the stations. Evaluation of the model performance for each form of T-NO$_3^-$ will be required in terms of gas-aerosol partitioning (HNO$_3$ and NO$_3^-$) and observations of mass size distribution (for submicron NH$_4$NO$_3$ and super-micron NaNO$_3$) to identify the reasons for the discrepancies in surface concentrations and to improve the model performance for T-NO$_3^-$.

3.4 A hypothesis: possible influence of large sea salt particles (LSPs) on wet deposition near-the-coast (NC) stations

Notably, the simulated W-Na$^+$ deposition at the NC stations (Fig. 7h) was greatly underestimated (up to a factor of 30 at Station 3) compared to the observations, whereas the simulated and observed depositions were closer at the FC stations. The results in Fig. 7h raise questions regarding whether underestimation of the wet scavenging rate of Na$^+$ may be the sole reason for the discrepancy, because Na$^+$ concentrations at the FC stations were overestimated. However, this overestimation may not be the sole cause. First, the amount of wet deposition is not always related to the surface concentration because the precipitation process involves vertical transport and mixing of air pollutants and is, therefore, affected by both upper air and near-surface constituents. Second, the RMSEs were always smaller or comparable to modeled or observed averages, except for the wet deposition of Na$^+$ at the NC stations (52.2 mmol m^{-2}), which was significantly larger than the observed and modeled averages (16.4 and 1.38 mmol m^{-2}, respectively). Nevertheless, it is not possible to explain the discrepancy because the current model configuration is not appropriate to simulate it: the horizontal grid resolution is too coarse to resolve the NC stations, and the sea salt emission in the surf zone is not considered. The current off-line coupling framework together with the coarse grid resolution is not suitable for resolving the cloud microphysics process or for tracking the aerosols involved in it.

Another reason may explain the large underestimation in the Na$^+$ wet deposition. We presumed here that large sea salt particles (LSPs; diameter > 10 μm) contributed substantially to the large values of [W-Na$^+$] at the NC stations. While the wet-only precipitation sampler can collect any size of the droplets during precipitation events, the aerosol sampler cannot. We stated that the FP method efficiently collected particles of up to diameters of 10 μm, but the collection efficiency could be substantially lower for particles larger than 10 μm. This lower efficiency is due to the flow rate being too low (1 l min^{-1}) for LSPs, which have a large downward velocity

to reach the bottom of the pack (see configuration of the instruments in EANET "Technical Documents for Filter Pack Method in East Asia" at http://www.eanet.cc/product.html). With a flow rate of 1 l min^{-1} and with a filter diameter of 47 mm, the average flow rate is approximately 0.2 cm s^{-1} ($= v/\pi d^2$; $d = 47$ mm, $v = 1$ l min^{-1}). This speed is the case for pack without the filter; thus, the actual flow rate should be lower than this. The gravitational settling velocity of particles with $D = 10$ μm is approximately 1 cm s^{-1}; thus, the collection efficiency of particles larger than 10 μm could be lower for the current settings. This result is consistent with the fact that modeled aerosol Na$^+$ agreed quantitatively with the observations at NC stations.

Coarse-mode particles (diameter ∼ several μm) are produced by bubbles bursting within whitecaps (an indirect process), whereas LSPs are produced when strong winds disrupt wave crests and tear off drops of spumes (a direct process) (Monahan, 1971). The diameter of sea salt particles produced via the direct process could be larger than 100 μm. The surface wind speed at 10 m elevation needs to be > 10 m s^{-1} for winds to tear off the crests over the open ocean. Some of the NC stations were located on rocky cliffs by the ocean. Waves hitting the cliffs also produced substantial amounts of LSPs and may have contributed to the effects. LSPs are also produced under lower wind speed cases in the surf zone, and the amounts could be substantially higher than those in the open ocean (de Leeuw et al., 2000). Because such LSPs are not long lived in the air, they are not transported over long distances; thus, the direct process is not usually considered in regional- and global-scale transport models (Gong et al., 1997). Because the dry deposition velocities of LSPs and their collection efficiency by hydrometeors are high, LSPs are efficiently removed from the air and collected in the wet-only deposition samples.

Suto et al. (2010) estimated that depositional mass fluxes of sea salt particles of whole size ranges (coarse mode plus LSPs) decreased by one order of magnitude at distances of several kilometers from Tokyo Bay and by two orders of magnitude at distances of several tens of kilometers from the coast. LSPs can be transported approximately 1–10 km horizontally from the coast, indicating that the horizontal representation of W-Na$^+$ and W-Cl$^-$, the wet deposition components derived from sea salt, is limited by the traveling distance of LSPs.

More than half of NO$_3^-$ (and even > 90 % at Hedo) is thought to be internally mixed with coarse-mode sea salt to form NaNO$_3$ at Japanese EANET stations located over the ocean (Kajino and Kondo, 2011; Kajino et al., 2012). If the scavenging rate of coarse-mode sea salt in the model was underestimated, then [W-NO$_3^-$] would also be underestimated. However, the differences between [W-NO$_3^-$] and [T-NO$_3^-$] are much smaller than those between [W-Na$^+$] and [Na$^+$], which is one order of magnitude or more (Fig. 7f and h). Because LSPs are short lived, they remain pure and are not

mixed with NO_3^-. Therefore, our presumption is consistent with the result that only the modeled [W-Na$^+$] at NC stations was significantly underestimated. The wet deposition processes are not the same between T-NO$_3^-$ and Na$^+$, because HNO$_3$ gas dissolved in precipitation may also contribute to [W-NO$_3^-$]. Nevertheless, the feature is the same when the concentration of HNO$_3$ gas was extremely low under cold winter temperatures.

3.5 Estimating changes in pH of precipitation induced by large sea salt particles (LSPs)

EANET has been monitoring the pH of precipitation in Asia since 2001. There are currently 12 stations in Japan, and half of them are situated very close to the coast. The pH of sea water is approximately 8, which is much higher than that of precipitation in Japan (pH $4 \sim 5$). If our hypothesis presumed in Sect. 3.4 is true, the short-lived LSPs could raise the pH values of precipitation in Japan, and those values were not representative of precipitation for all of Japan (representing only the traveling distance of LSPs, 1–10 km). However, because the salinity of precipitation is much lower than that of sea water (approximately three orders of magnitude, estimated from the averages of Table 2), the pH of the diluted seawater becomes almost 7 and, thus, should not affect the pH of precipitation substantially. We proved this fact from the following calculation.

We used the method of Walcek and Taylor (1986) to estimate the effects of LSPs on precipitation pH by iteratively solving the following charge-balance equation for the concentrations of positive and negative ions:

$$
\begin{aligned}
[H^+] &+ [NH_4^+] + 2([Ca^{2+}] + [Mg^{2+}]) + [Na^+] + [K^+] \\
&= [OH^-] + [HSO_3^-] \qquad\qquad (3) \\
&\quad + [Cl^-] + [HCO_3^-] + 2([SO_4^{2-}] \\
&\quad + [CO_3^{2-}] + [SO_3^{2-}]) + [NO_3^-] + [HSO_4^-].
\end{aligned}
$$

We assumed the chemical components of sea water following Song and Carmichael (2001), CO$_2$ mixing ratio at 360 ppm, ocean surface salinity of 35, and obtained a consistent value of sea water pH (8.2). To assess the applicability of the method, we compared the simulated pH of daily precipitation using the measured chemical compositions ([SO$_4^{2-}$], [NO$_3^-$], [Cl$^-$], [NH$_4^+$], [Ca^{2+}], [Mg^{2+}], [Na$^+$], and [K$^+$]) with the measured pH at the EANET NC stations (Stations 1–6). For the simulation, we assumed the initial gas phase concentration of HNO$_3$, HCl, and NH$_3$ to be equilibrated with the measured [NO$_3^-$], [Cl$^-$], and [NH$_4^+$] at the measured pH. The simulated median pH (4.94) was slightly higher than the observed pH (4.82), but we obtained a high R^2 (0.83) and low RMSE (0.37). The slope of a regression line that fit the observed and simulated pH values (Fig. 8a), and had zero intercept, was 1.042.

Based on the previous discussion and together with Fig. 7h, it seems reasonable to assume that LSPs accounted
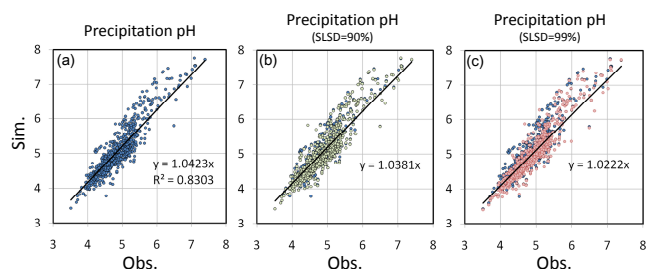

Fig. 8. Scatter diagrams of daily precipitation pH at NC stations, (x-axis) observed and (y-axis) calculated using **(a)** observed chemical compositions (blue), **(b)** with 90 % of the components derived from sea salt excluded (green), and **(c)** with 99 % of the components derived from sea salt excluded (pink).

for 90 % of the total sea salt components in precipitation at the NC stations (distance < 1 km). The calculated pH of the precipitation decreased slightly when we excluded LSP effects (green points in Fig. 8b). Table 3 summarizes the average, 75th percentile, median, and 25th percentile values of observed and simulated daily precipitation pH at the NC stations. The average pH was not an arithmetic average of daily pH values, but instead was equated to minus the common logarithm of the average of the daily [H$^+$] concentrations. The simulated effect of 90 % LSP contamination of the sea salt resulted in an increase in pH by 0.014, from 4.69 to 4.71 on average. This increment is very small and indeed much smaller than the RMSE (0.37) between the simulated and observed pH. Even if we assumed that LSPs accounted for 99 % of the total sea salt components in precipitation, the effect on pH was only approximately 0.1 (Fig. 8c, Table 3). Therefore, the proximity to the coast of the remote EANET stations on islands or isolated capes does not seriously confound the monitoring of background levels of precipitation pH. Nevertheless, careful attention is needed as the substantial contribution of LSPs may prohibit accurate determination of [W-nss-SO$_4^{2-}$] or [W-nss-Ca^{2+}] in precipitation by subtracting the huge [W-Na$^+$] term in Eqs. (1) and (2).

4 Conclusions

We conducted a regional-scale simulation using an aerosol chemical transport model (RAQM2, Kajino et al., 2012) with time-varying lateral and upper boundary concentrations of gaseous species that were predicted with a global stratospheric and tropospheric chemistry-climate model (MRI-CCM2, Deushi and Shibata, 2011). The current model system is referred to as the MRI–Passive-tracers Model system for atmospheric Chemistry (MRI-PM/c). We demonstrated its performance with respect to major anthropogenic and natural inorganic components, SO$_4^{2-}$, NH$_4^+$, NO$_3^-$, Na$^+$ and Ca^{2+} in the air as well as in rain and snow precipitation. Statistical analysis showed that approximately 40–50 % and

Table 3. Statistical values of observed and simulated daily precipitation pH at all the NC stations (Stations 1–6).

	Average[a]	75 percentile	Median	25 percentile
Observed pH	4.60	5.18	4.82	4.49
Simulated pH	4.71	5.36	4.94	4.59
Simulated pH (LSP = 90 %)[b]	4.69	5.36	4.93	4.57
Simulated pH (LSP = 99 %)[c]	4.60	5.28	4.87	4.51
ΔpH (LSP = 90 %)[b]	0.014	0.027	0.0096	0.0024
ΔpH (LSP = 99 %)[c]	0.10	0.14	0.033	0.0062

[a] Minus the common logarithm of the average of the daily $[H^+]$. [b] Simulation with observed chemical compositions but excluding 90 % of the components originated from sea salt. [c] Simulation with observed chemical compositions but excluding 99 % of the components originated from sea salt.

70–80 % of simulated concentration and wet deposition of SO_4^{2-}, NH_4^+, NO_3^- and Ca^{2+} are within factors of 2 and 5 of the observations, respectively. The performance in the simulation of the wet deposition amount is nevertheless noteworthy, because there had been differences of one to two orders of magnitude among several regional-scale models for simulating monthly mean values of the wet deposition of SO_4^{2-}, NH_4^+ and NO_3^- (Wang et al., 2008).

The prediction of the sea-salt originated component Na^+ was not successful at near-coastal stations (where the distance from the coast was from 150 to 700 m), because the model grid resolution ($\Delta x = 60$ km) is too coarse to resolve it. We found a large underestimation of Na^+ (up to a factor of 30) in precipitation. The RMSEs were always smaller or comparable to modeled or observed averages, except for the wet deposition of Na^+ (52.2 mmol m^{-2}), which was significantly larger than the observed and modeled averages (16.4 and 1.38 mmol m^{-2}, respectively). We hypothesized that this result was most likely due to the contribution of short-lived large sea salt particles (LSPs; diameters larger than 10 µm) in rainwater samples. Because of the presence of these droplets, measurements of the compositions of wet deposition derived from sea salt, such as Na^+ and Cl^-, would not be representative beyond the horizontal traveling distance of LSPs. However, we calculated the effects of LSPs on precipitation pH to be very low, a change of approximately +0.014 on average, based on the assumption that LSPs were the source of 90 % of the components of sea salt in precipitation. Even if LSPs accounted for 99 % of total sea salt, the change of pH would be only approximately +0.1. Therefore, the proximity to the coast of the remote EANET stations is not a serious problem for monitoring background levels of precipitation pH.

The discrepancy between the simulated and observed surface [T-NO_3^-] values was greater than it was for any other components. Nitrates exist in various forms in the air, including HNO_3 gas, NH_4NO_3 in submicron particles, and $NaNO_3$ in coarse-mode sea salt particles. Dry and wet deposition rates might be substantially different among these three forms. To improve the simulation of [T-NO_3^-], we need to assess the model performance for each form of nitrate by comparing the simulated results with measurements of gas-aerosol partitioning and of mass size distributions of nitrate.

Finally, online coupling of regional-scale meteorology with a chemical transport model with finer grid resolutions will be essential for better simulation of the processes of wet deposition. Although RAQM2 could "diagnose" autoconversion and accretion rates with a mixed-phase parameterization of cloud microphysics, these rates were based on environmental and microphysical parameters with 60 km of grid spacing at a time resolution of 1 h, which is too coarse and too long for the special and temporal scale of dynamic and microphysical processes in clouds.

References

Abdul-Razzak, H. and Ghan, S. J.: A parameterization of aerosol activation, 2. Multiple aerosol typles, J. Geophys. Res., 105, 6837–6844, 2000.

Bond, T. C., Streets, D. G., Yarber, K. F., Nelson, S. M., Woo, J.–H., and Klimont, Z.: A technology-based global inventory of black and organic carbon emission from combustion, J. Geophys. Res., 109, D14203, doi:10.1029/2003JD003697, 2004.

Carmichael, G. R., Sakurai, T., Streets, D., Hozumi, Y., Ueda, H., Park, S. U., Fung, C., Han, Z., Kajino, M., Engardt, M., Bannet, C., Hayami, H., Sartelet, K., Holloway, T., Wang, Z., Kannari, A., Fu, J., Matsuda, K., Thongboonchoo, N., and Amann, M.: MICS-Asia II: the model intercomparison study for Asia phase II methodology and overview of findings, Atmos. Environ., 42, 3468–3490, 2008.

Clarke, A. D., Owens, S. R., and Zhou, J.: An ultrafine sea-salt flux from breaking waves: Implications for cloud condensation nuclei in the remote marine atmosphere, J. Geophys. Res., 111, D06202, doi:10.1029/2005JD006565, 2006.

de Leeuw, G., Neele, F. P., Hill, M., Smith, M. H., and Vignati, E.: Production of sea spray aerosol in the surf zone, J. Geophys. Res., 105, 29397–29409, 2000.

Deushi, M. and Shibata, K.: Development of an MRI Chemistry-Climate Model ver.2 for the study of tropospheric and straro-spheric chemistry, Papers in Meteor. Geophys., 62, 1–46, 2011.

DOE, 1994: Handbook of methods for the analysis of the various parameters of the carbon dioxide system in sea water, Version 2, edited by: Dickson, A. G. and Goyet, C., ORNL/CDIAC-74, 1994.

Giglio, L., Randerson, J. T., van der Werf, G. R., Kasibhatla, P. S., Collatz, G. J., Morton, D. C., and DeFries, R. S.: Assessing variability and long-term trends in burned area by merging multiple satellite fire products, Biogeosciences, 7, 1171–1186, doi:10.5194/bg-7-1171-2010, 2010.

Gong, S. L., Barrie, L. A., and Blanchet, J.-P.: Modeling sea salt aerosols in the atmosphere, 1. Model development, J. Geophys. Res., 102, 3805–3818, 1997.

Guenther, A., Karl, T., Harley, P., Wiedinmyer, C., Palmer, P. I., and Geron, C.: Estimates of global terrestrial isoprene emissions using MEGAN (Model of Emissions of Gases and Aerosols from Nature), Atmos. Chem. Phys., 6, 3181–3210, doi:10.5194/acp-6-3181-2006, 2006.

Han, Z., Ueda, H., Matsuda, K., Zhang, R., Arao, K., Kanai, Y., and Hasome, H.: Model study on particle size segregation and deposition during Asian dust events in March 2002, J. Geophys. Res., 109, D19205, doi:10.1029/2004JD004920, 2004.

Han, Z., Sakurai, T., Ueda, H., Carmichael, G. R., Streets, D., Hayami, H., Wang, Z., Holloway, T., Engardt, M., Hozumi, Y., Park, S. U., Kajino, M., Sartelet, K., Fung, C., Bennet, C., Thongboonchoo, N., Tang, Y., Chang, A., Matsuda, K., and Amann, M.: MICS-Asia II: Model intercomparison and evalution of ozone and relevant species, Atmos. Environ., 42, 3491–3509, 2008.

Hayami, H., Sakurai, T., Han, Z., Ueda, H., Carmichael, G. R., Streets, D., Holloway, T., Wang, Z., Thongboonchoo, N., Engardt, M., Bennet, C., Fung, C., Chang, A., Park, S. U., Kajino, M., Sartelet, K., Matsuda, K., and Amann, M.: MICS-Asia II: Model intercomparison and evalution of particulate sulfate, nitrate and ammonium, Atmos. Environ., 42, 3510–3527, 2008.

Kajino, M.: MADMS: Modal Aerosol Dynamics model for multiple Modes and fractal Shapes in the free-molecular and near-continuum regimes, J. Aerosol Sci., 42, 224–248, 2011a.

Kajino, M.: Development of an efficient but accurate new dynamics model to predict a variety of atmospheric aerosol properties and their elemental processes, Earozoru Kenkyu, 26, 296–306, 2011b (in Japanese).

Kajino, M. and Kondo, Y.: EMTACS: Development and regional-scale simulation of a size, chemical, mixing type, and soot shape resolved atmospheric particle model, J. Geophys. Res., 116, D02303, doi:10.1029/2010JD015030, 2011.

Kajino, M. and Ueda, H.: Chapter 2, Secondary Acidification, Monitoring, Control and Effects of Air Pollution, edited by: Chmielewski, A. G., In Tech Open Access Publisher, ISBN:978-953-307-526-6, 15–38, 2011.

Kajino, M., Ueda, H., Satsumabayashi, H., and Han, Z.: Increase in nitrate and chloride deposition in East Asia due to increased sulfate associated with the eruption of Miyakejima Volcano, J. Geophys. Res., 110, D18203, doi:10.1029/2005JD005879, 2005.

Kajino, M. and Ueda, H.: Chapter 2.6 Increase in nitrate deposition as a result of sulfur dioxide emission increase in Asia: Indirect acidification, Develop. Environ. Sci., 6, 134–143, 2007.

Kajino, M., Ueda, H., and Nakayama, S.: Secondary acidification: Changes in gas-aerosol partitioning of semivolatile nitric acid and enhancement of its deposition due to increased emission and concentration of SO_x, J. Geophys. Res., 113, D03302, doi:10.1029/2007JD008635, 2008.

Kajino, M., Inomata, Y., Sato, K., Ueda, H., Han, Z., An, J., Katata, G., Deushi, M., Maki, T., Oshima, N., Kurokawa, J., Ohara, T., Takami, A., and Hatakeyama, S.: Development of an aerosol chemical transport model RAQM2 and predictions of Northeast Asian aerosol mass, size, chemistry, and mixing type, Atmos. Chem. Phys. Discuss., 12, 13405–13456, doi:10.5194/acpd-12-13405-2012, 2012.

Kuang, C., McMurry, P. H., McCormick, A. V., and Eisele, F. L.: Dependence of nucleation rates on sulfuric acid vapor concentration in diverse atmospheric locations. J. Geophys. Res. 113, D10209, doi:10.1029/2007JD009253, 2008.

Kurokawa, J., Ohara, T., Uno, I., Hayasaki, M., and Tanimoto, H.: Influence of meteorological variability on interannual variations of springtime boundary layer ozone over Japan during 1981–2005, Atmos. Chem. Phys., 9, 6287–6304, doi:10.5194/acp-9-6287-2009, 2009.

Lin, Y.–L., Farley, R. D., and Orville, H. D.: Bulk parameterization of the snow field in a cloud model, J. Clim. Appl. Meteorol., 22, 1065–1092, 1983.

Lohmann, U. and Diehl, K.: Sensitivity studies of the importance of dust ice nuclei for the indirect aerosol effect on stratiform mixed-phase clouds, J. Atmos. Sci., 63, 968–982, 2010.

Monahan, E. C.: Oceanic whitecaps, J. Phys. Oceanogr., 1, 139–144, 1971.

Ohara, T., Akimoto, H., Kurokawa, J., Horii, N., Yamaji, K., Yan, X., and Hayasaka, T.: An Asian emission inventory of anthropogenic emission sources for the period 1980–2020, Atmos. Chem. Phys., 7, 4419–4444, doi:10.5194/acp-7-4419-2007, 2007.

Oliver, J. G. J. and Berdowski, J. J. M.: Global emission sources and sinks, in: The Climate System, edited by: Berdowski, J., Guicherit, R., and Heij, B. J., A. A. Balkema, Lisse, Netherlands, 33–78, 2001.

Oliver, J. G. J., Bouwman, A. F., Berdowski, J. J. M., Veldt, C., Bloos, J. P. Jp, Visschedijk, A. J. H., Van der Maas, C. W. M., and Zandveld, P. Y. J.: Sectoral emission inventories of greenhouse gases for 1990 on a per country basis as well as on 1×1, Environ. Sci. Policy, 2, 241–263, doi:10.1016/S1462-9011(99)00027-1, 1999.

Saide, P. E., Spak, S. N., Carmichael, G. R., Mena-Carrasco, M. A., Yang, Q., Howell, S., Leon, D. C., Snider, J. R., Bandy, A. R., Collett, J. L., Benedict, K. B., de Szoeke, S. P., Hawkins, L. N., Allen, G., Crawford, I., Crosier, J., and Springston, S. R.: Evaluating WRF-Chem aerosol indirect effects in Southeast Pacific marine stratocumulus during VOCALS-REx, Atmos. Chem. Phys., 12, 3045–3064, doi:10.5194/acp-12-3045-2012, 2012.

Saito, K., Ishida, J., Aranami, K., Hara, T., Segawa, T., Narita, M., and Honda, Y.: Nonhydrostatic atmospheric models and operational development at JMA, J. Meteorol. Soc. Jpn, 85B, 271–304, doi:10.2151/jmsj.85B.271, 2007.

Song, C.-H. and Carmichael, G. R.: A three-dimensional modeling investigation of the evolution processes of dust and sea-salt particles in east Asia, J. Geophys. Res., 106, 18131–18154, 2001.

Skamarock, W. C., Klemp, J. B., Dudhia, J., Gill, D. O., Barker, D. M., Duda, M. G., Huang, X. Y., Wang, W., and Powers, J. G.: A description of the advanced research WRF version 3, Tech. Note, NCAR/TN~475+STR, Natl. Cent. for Atmos. Res., Boulder, Colo., 125 pp., 2008.

Suto, H. Hattori, Y., Hirakuchi, H., and Kihara, N.: Study of estimation of salt deposition with numerical simulation of sea salt particle transport (Part 4) – Application of estimation method for wide area distribution of sea salt to the Kanto region, Civil Engineering Research Laboratory Rep. No. N10006, CRIEPI, ISBN978-4-7983-0412-0, 2010 (in Japanese).

Tang, Y., Carmichael, G. R., Kurata, G., Uno, I., Weber, R. J., Song, C.-H., Guttikunda, S. K., Woo, J.–H., Streets, D. G., Wei, C., Clarke, A. D., Huebert, B., and Anderson, T. L.: Impacts of dust on regional tropospheric chemistry during the ACE-Asia experiment: A model study with observations, J. Geophys. Res., 109, D19S21, doi:10.1029/2003JD003806, 2004.

Walcek, C. J. and Taylor, G. R.: A theoretical method for computing vertical distributions of acidity and sulfate production within cumulus clouds, J. Atmos. Sci., 43, 339–355, 1986.

Wang, Z., Xie, F., Sakurai, T., Ueda, H., Han, Z., Carmichael, G. R., Streets, D., Engardt, M., Holloway, T., Hayami, H., Kajino, M., Thongboonchoo, N., Bennet, C., Park, S. U., Fung, C., Chang, A., Sartelet, K., Amann, M.: MICS-Asia II: Model intercomparison and evaluation of acid deposition, Atmos. Environ., 42, 3528–3542, 2008.

Zhang, Q., Streets, D. G., Carmichael, G. R., He, K. B., Huo, H., Kannari, A., Klimont, Z., Park, I. S., Reddy, S., Fu, J. S., Chen, D., Duan, L., Lei, Y., Wang, L. T., and Yao, Z. L.: Asian emissions in 2006 for the NASA INTEX-B mission, Atmos. Chem. Phys., 9, 5131–5153, doi:10.5194/acp-9-5131-2009, 2009.